REFERENCES

[1] B. Bianco and S. Ridella, "Nonconventional transmission zeros in distributed rectangular structures," *IEEE Trans. Microwave Theory Tech.*, vol. MTT-20, pp. 297–303, May 1972.

[2] G. Kompa, "S-Matrix computation of microstrip discontinuities with a planar waveguide model," *Arch. Elek. Übertragung*, vol. 30, pp. 58–64, Feb. 1976.

[3] G. Kompa and R. Mehran, "Planar waveguide model for calculating microstrip components," *Electron. Lett.*, vol. 11, pp. 459–460, Sept. 1975.

[4] T. Okoshi, Y. Uehara, and T. Takeuchi, "The segmentation method—An approach to the analysis of microwave planar circuits," *IEEE Trans. Microwave Theory Tech.*, vol. MTT-24, pp. 662–668, Oct. 1976.

[5] T. Okoshi and T. Miyoshi, "The planar circuit—An approach to microwave integrated circuitry," *IEEE Trans. Microwave Theory Tech.*, vol. MTT-20, pp. 245–252, Apr. 1972.

[6] P. Silvester, "Finite-element analysis of planar microwave networks," *IEEE Trans. Microwave Theory Tech.*, vol. MTT-21, pp. 104–108, Feb. 1973.

[7] G. D'Inzeo, F. Giannini, and R. Sorrentino, "Theoretical and experimental analysis of non-uniform microstrip lines in the frequency range 2–18 GHz," in *Proc. of 6th European Microwave Con.* (Rome, Italy) pp. 627–631, 1976.

[8] W. Menzel and I. Wolff, "A method for calculating the frequency-dependent properties of microstrip discontinuities," *IEEE Trans. Microwave Theory Tech.*, vol. MTT-25, pp. 107–112, Feb. 1977.

[9] I. Wolff and N. Knoppik, "Rectangular and circular microstrip disk capacitors and resonators," *IEEE Trans. Microwave Theory Tech.*, vol. MTT-22, pp. 857–864, Oct. 1974.

[10] G. Kompa, "Excitation and propagation of higher modes in microstrip discontinuities," presented at *Proc. of 3th European Microwave Conf.*, Brussels, 1973.

[11] I. Wolff, G. Kompa, and R. Mehran, "Calculation methods for microstrip discontinuities and T-junctions," *Electron. Lett.*, vol. 8, pp. 177–179, Apr. 1972.

[12] B. Bianco, M. Granara, and S. Ridella, "Comments on the existence of transmission zeros in microstrip discontinuities," *Alta Frequenza*, vol. XLI, pp. 533E–534E, Nov. 1972.

[13] B. Bianco, M. Granara, and S. Ridella, "Filtering properties of two-dimensional lines' discontinuities," *Alta Frequenza*, vol. XLII, pp. 140E–148E, July 1973.

[14] K. Kurokawa, *An Introduction to the Theory of Microwave Circuits*. New York: Academic Press, 1969, ch. 4.

[15] P. M. Morse and H. Feshbach, *Methods of Theoretical-Physics*, vol. I. New York: McGraw-Hill, 1953, ch. 6, pp. 716–719.

[16] H. A. Wheeler, "Transmission-line properties of parallel wide strips separated by a dielectric sheet," *IEEE Trans. Microwave Theory Tech.*, vol. MTT-13, pp. 172–185, Mar. 1965.

[17] M. V. Schneider, "Microstrip lines for microwave integrated circuits," *Bell Syst. Tech. J.*, vol. 48, pp. 1421–1444, May 1969.

[18] ——, "Microstrip dispersion," *Proc. Inst. Elect. Electron. Engrs.*, vol. 60, pp. 144–146, 1972.

[19] G. N. Tsandoulas and W. J. Ince, "Modal inversion in circular waveguides—Part I: Theory and phenomenology," *IEEE Trans. Microwave Theory Tech.*, vol. MTT-19, pp. 386–392, Apr. 1971.

[20] F. Giannini, P. Maltese, and R. Sorrentino, "Liquid crystal technique for field detection in microwave integrated circuitry," *Alta Frequenza*, vol. XLVI, pp. 80E–88E, Apr. 1977.

[21] S. Akhtarzad and P. B. Johns, "Three-dimensional transmission-line matrix computer analysis of microstrip resonators," *IEEE Trans. Microwave Theory Tech.*, vol. MTT-23, pp. 990–997, Dec. 1975.

[22] R. Jansen, "High-order finite element polinomials in the computer analysis of arbitrarily shaped microstrip resonators," *Arch. Elek. Übertragung*, vol. 30, pp. 71–79, Feb. 1976.

[23] T. Itoh, "Analysis of microstrip resonators," *IEEE Trans. Microwave Theory Tech.*, vol. MTT-22, pp. 946–951, Nov. 1974.

Analysis of Planar Disk Networks

RENÉ R. BONETTI AND PLINIO TISSI

Abstract—**The impedance matrix of a disk n-port is determined with fringing fields at the disk edge included in the analysis. The theory is valid for both stripline and microstrip geometries and is also applicable to magnetic substrates. A simple quasi-static approximation to the disk capacitance is obtained. Applicability to numerical design is exemplified with the search for transmission zeros in a reciprocal 2 port. Experimental results are presented for the 1-port and 2-port disks.**

I. INTRODUCTION

PLANAR NETWORK theory is becoming a powerful tool for the design of microwave integrated circuits [1]–[4]. When compared to other physical structures, planar networks offer the designer considerable freedom, due not only to their size and shape but also to the large variety of devices realizable with simple geometries.

A very simple shape, the disk, has already proven very useful for the realization of junction circulators and presents interesting possibilities for other devices.

Well known theories for disk networks on magnetic substrate [5]–[7] make use of the edge magnetic wall (EMW) as a boundary condition at the disk edge and, therefore, exterior fields are not included in the analysis. With respect to this problem we quote Bosma [8]: "It is the unsolved problem of the fringing field that makes numerical design of circulators not yet very spectacular." Furthermore, in a recent paper by de Santis [9] transitions from volume modes to edge guided modes were shown to be strongly influenced by these fields.

Manuscript received March 1, 1977; revised September 22, 1977. This work was supported by contract FINEP-271-CT.

The authors are with the Instituto de Pesquisas Espaciais, Conselho Nacional de Desenvolvimento Cientifico e Tecnológico, São José dos Campos, SP, Brazil.

0018-9480/78/0700-0471$00.75

This work presents a theory for the general multiport disk, which includes an analytical treatment of the fringing fields and is also applicable to magnetic substrates. As a consequence, it represents a sound basis for the accurate design of MIC devices such as resonators, filters, and circulators. The theory lends itself well to computational implementation and numerical synthesis since the eigenfunctions are computed independently of the number, positions, and widths of the ports. Consequently, the search for optimum port parameters is performed by means of relatively simple algorithms.

Examples of applications are given for isotropic resonators and filters.[1]

II. Formulation of Geometry and Basic Hypotheses

The network consists of a highly conducting disk, placed either between (Fig. 1(a) and (b)) or above (Fig. 1(c) and (d)) a magnetic substrate, extending only to the disk edge, and magnetized in the z direction. The outer dielectric extends to infinity, or is bounded along a circular contour, by an electric or magnetic wall. The geometry in the z direction is one of the two types described in Fig. 1. The disk is coupled to K ports, each spanning an angle $2\psi_i$ $(i=1,2,\cdots,K)$ at the edge, in such a way that no two ports have any points in common (Fig. 2). Each port is connected to a line, which is inbedded in the homogeneous outer dielectric.

As in previous works [5]–[7] the azimuthal component of the RF magnetic field is assumed as constant along the ports and only TM modes relative to the z axis are considered. In the microstrip cases (Fig. 1(c) and (d)) the exterior fields $(R_1<r<R_2)$ are limited from above by a magnetic wall parallel to the ground plane at $z=h$. Coupling between the exterior fields and the strip or microstrip lines is neglected. The operating frequency is restricted by

$$f<\left[2h(\mu_1\epsilon_1)^{1/2}\right]^{-1} \tag{1}$$

which is the condition for the z independent modes to be dominant in the magnetic material (see A7).

The stripline disk thickness is assumed to obey the condition $t\ll h$ (see Fig. 1). Based on this, boundary conditions at $h<z<h+t$ and $r=R_1$ are not considered.

III. Formal Solution of the Field Problem

The general expressions for the z independent modes in the magnetic material are the well-known expansions [5]:

$$E_z^{(1)}(r,\phi)=\sum_n M_n J_n(k_1 r)e^{-jn\phi} \tag{2}$$

$$H_\phi^{(1)}(r,\phi)=-jY_e\sum_n M_n F_n(k_1 r,\kappa/\mu)e^{-jn\phi} \tag{3}$$

$$H_r^{(1)}(r,\phi)=Y_e\sum_n M_n\left[\frac{nJ_n(k_1 r)}{k_1 r}-\frac{\kappa}{\mu}J_n'(k_1 r)\right]e^{-jn\phi} \tag{4}$$

[1]A second paper, including application to circulators, is in preparation.

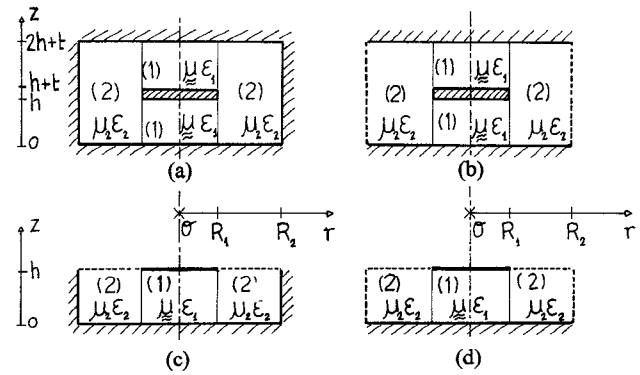

Fig. 1. Cross section of stripline disk geometry bounded by either an electric (a) or magnetic (b) wall at $r=R_2$, same for the microstrip disk (c), and (d), respectively.

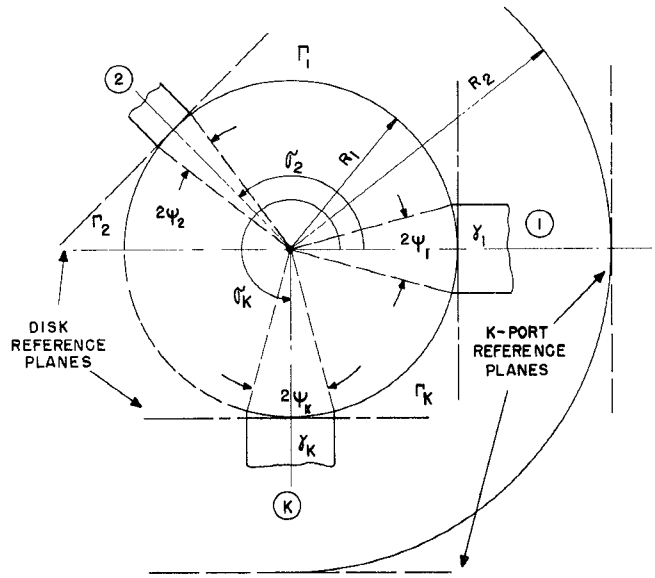

Fig. 2. Conductor disk geometry and reference planes.

where

$$F_n(k_1 r,\kappa/\mu)=J_n'(k_1 r)-\frac{\kappa}{\mu}\cdot\frac{nJ_n(k_1 r)}{k_1 r}$$

$$Y_e=(\epsilon_1/\mu_1)^{1/2}.$$

The main steps in the derivation of the eigenfunctions for the outer fields are given in the Appendix. In terms of those functions, the fields between consecutive strips can be written as[2]

$$E_z^{(2)}(r,\phi,z)=\sum_n\sum_m A_{nm}C_n(k_2 r)\cos\beta_2 z\cdot e^{-jn\phi} \tag{5a}$$

$$E_r^{(2)}(r,\phi,z)=-\sum_n\sum_m A_{nm}\beta_2 k_2^{-2}C_n'(k_2 r)\sin\beta_2 z\cdot e^{-jn\phi} \tag{5b}$$

$$E_\phi^{(2)}(r,\phi,z)=j\sum_n\sum_m A_{nm}\beta_2(k_2^2 r)^{-1}C_n(k_2 r)\sin\beta_2 z\cdot ne^{-jn\phi} \tag{5c}$$

[2]In order to write general expressions for the fields below and above cuttoff the symbol C_n' here means derivative with respect to the variable r. For simplicity, k_2 and β_2 stand for k_{2m} and β_{2m}, respectively.

TABLE I
RADIAL EIGENFUNCTIONS $C_n(k_2r)$

Geometry of Fig. 1	$\omega(\mu_2\epsilon_2)^{1/2} < \beta_2$	$\omega(\mu_2\epsilon_2)^{1/2} > \beta_2$
(a), (c)	$K_n(jk_2r) - \frac{K_n(jk_2R_2)}{I_n(jk_2R_2)} I_n(jk_2r)$	$J_n(k_2r) - \frac{J_n(k_2R_2)}{Y_n(k_2R_2)} Y_n(k_2r)$
(b), (d)	$K_n(jk_2r) - \frac{K_n'(jk_2R_2)}{I_n'(jk_2R_2)} I_n(jk_2r)$	$J_n(k_2r) - \frac{J_n'(k_2R_2)}{Y_n'(k_2R_2)} Y_n(k_2r)$

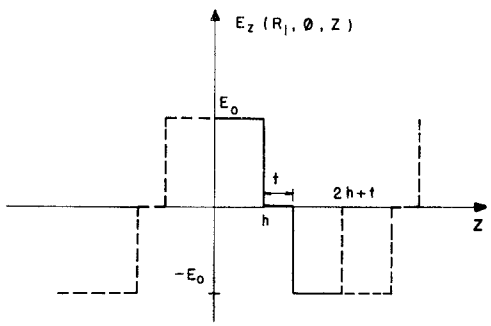

Fig. 3. Behavior of z component of electric field at the disk edge for the stripline disk (first depth mode only).

$$H_r^{(2)}(r,\phi,z)=\omega\epsilon_2\sum_n\sum_m A_{nm}(k_2^2r)^{-1}C_n(k_2r)\cos\beta_2 z\cdot ne^{-jn\phi} \tag{5d}$$

$$H_\phi^{(2)}(r,\phi,z)=-j\omega\epsilon_2\sum_n\sum_m A_{nm}k_2^{-2}C_n'(k_2r)\cos\beta_2 z\cdot e^{-jn\phi} \tag{5e}$$

where the eigenfunctions C_n are defined in Table I for the two different boundary conditions at $r=R_2$, relative to the geometries of Fig. 1.

The relationship between the two sets of mode coefficients M_n and A_{nm} will be obtained from the continuity of E_z at the edge of the disk:

$$E_z^{(1)}(R_1,\phi)+(\text{higher order depth modes})=E_z^{(2)}(R_1,\phi,z) \tag{6}$$

for $\phi\in\Gamma_i$ $(i=1,2,\cdots,k)$, and $0<z<2h+t$ (SD), $0<z<h$ (MD).

As an approximation to condition (6) the contribution of the higher order modes is neglected, so that the inner field is represented by (2) alone. This situation is sketched, for the stripline disk, in Fig. 3, where

$$E_0(\phi)=E_z^{(1)}(R_1,\phi). \tag{7}$$

In order to obtain a representation of the inner field in the whole interval $0<z<2h+t$, for this case, the function of Fig. 3 is expanded as

$$E_z^{(1)}(R_1,\phi,z)=2E_0(\phi)\sum_m\frac{(1-\cos m\pi)}{m}\cdot\sin\left(\frac{m\pi h}{2h+t}\right)\cos\left(\frac{m\pi z}{2h+t}\right). \tag{8}$$

For convenience, this same expansion with $t=0$ is used for the microstrip disk, since all that is required for this case is the field representation in the interval $0<z<h$.

Using (2), (7), and (8) condition (6) yields

$$A_{nm}=0, \qquad m \text{ even} \tag{9a}$$

$$A_{nm}=\frac{4}{m\pi}\sin\left(\frac{m\pi h}{2h+t}\right)\frac{J_n(k_1R_1)}{C_n(k_1R_1)}M_n, \qquad m \text{ odd} \tag{9b}$$

with $t=0$ in the microstrip geometry, to be understood hereafter.

The continuity of the tangential magnetic field component on the disk edge provides the relationship between the coefficients M_n and the port excitations. We have

$$H_\phi^{(1)}(R_1,\phi)+(\text{higher order depth modes})=H_\phi^{(2)}(R_1,\phi,z). \tag{10}$$

The integration of (10) along the disk depth yields

$$H_\phi^{(1)}(R_1,\phi)=\frac{1}{h}\int_0^h H_\phi^{(2)}(R_1,\phi,z)\,dz \tag{11}$$

since the contribution of the higher order depth modes, which vary as $\cos(m\pi z/h)$ (see Appendix), does not exist.

The integration is performed using the expansion (5e) by eliminating the coefficients A_{nm} through (9). The result is

$$H_\phi^{(1)}(R_1,\phi)=-2j\omega\epsilon_2R_1\sum_n M_nJ_n(k_1R_1)\Lambda_n e^{-jn\phi} \tag{12}$$

in which we define the fringing function of order n as

$$\Lambda_n\equiv\Lambda_n(\Omega,\hat{R}_1,\hat{R}_2,\hat{t})=\frac{2}{2+\hat{t}}\sum_{m=1,3\cdots}^{\infty}\left[\frac{\sin\beta_2h}{\beta_2h}\right]^2\frac{\hat{R}_1}{\chi^2}\frac{C_n'(\chi)}{C_n(\chi)} \tag{13}$$

with

$$\Omega=\omega h(\mu_2\epsilon_2)^{1/2}$$

$$\chi^2=k_2^2R_1^2=\left[\Omega^2-\left(\frac{m\pi}{2+\hat{t}}\right)^2\right]\hat{R}_1^2.$$

We point out that the tangential magnetic field component is given by (12) only in the sectors Γ_i and is defined at the inner end of the lines on γ_i by the port excitation H_i. The inversion of expansion (3) yields

$$M_p=j(2\pi Y_eF_p)^{-1}\sum_{i=1}^{K}\cdot\left[\int_{\gamma_i}H_ie^{jp\phi}\,d\phi+\int_{\Gamma_i}H_\phi^{(1)}(R_1,\phi)e^{jp\phi}\,d\phi\right] \tag{14}$$

where $p=0,\pm1,\pm2,\cdots$.

Substituting (12) in this equation and defining

$$b_{pi}=\int_{-\psi_i}^{\psi_i}\exp[jp(\phi+\sigma_i)]\,d\phi \tag{15}$$

$$T_{np}=\sum_{i=1}^{K}\int_{\Gamma_i}\exp[j(p-n)\phi]\,d\phi \tag{16}$$

we obtain

$$F_p M_p - \frac{k_1 R_1}{\pi}\frac{\epsilon_2}{\epsilon_1}\sum_n \Lambda_n M_n T_{np} J_n(k_1 R_1) = \frac{j}{2\pi Y_e}\sum_{i=1}^{K} H_i b_{pi} \quad (17)$$

where $p = 0, \pm 1, \pm 2, \cdots$.

This set of equations allows the determination of the modal coefficients M_p for a general excitation of the disk ports when the fringing fields are taken into account. Due to the presence of the term $k_1 R_1$ one can expect that the influence of these fields will be stronger at higher frequencies.

IV. Impedance Matrix

In this section a relationship between the port voltages and currents at the disk reference planes is first derived followed by the determination of the impedance matrix of the K port.

To this end we introduce the following matrices:

$$\boldsymbol{m} = [\, M_{-N} \quad M_{-N+1} \quad \cdots \quad M_N \,]^t$$

$$\boldsymbol{\xi} = [\, H_1 \quad H_2 \quad \cdots \quad H_K \,]^t$$

$$\boldsymbol{v} = [\, V_1 \quad V_2 \quad \cdots \quad V_K \,]^t$$

$$\boldsymbol{i} = [\, I_1 \quad I_2 \quad \cdots \quad I_K \,]^t$$

$$\boldsymbol{\Lambda} = \mathrm{diag}[\, \Lambda_{-N}, \Lambda_{-N+1} \quad \cdots \quad \Lambda_N \,]$$

$$\boldsymbol{F} = \mathrm{diag}[\, F_{-N}, F_{-N+1} \quad \cdots \quad F_N \,]$$

$$\boldsymbol{J} = \mathrm{diag}[\, J_{-N}, J_{-N+1} \quad \cdots \quad J_N \,]$$

$$\boldsymbol{\Psi} = \mathrm{diag}[\, 1/\psi_1, 1/\psi_2 \quad \cdots \quad 1/\psi_K \,]$$

$$\boldsymbol{T} = \| T_{lj} \|_{\substack{j=-N,-N+1,\cdots N \\ l=-N,-N+1,\cdots N}}$$

$$\boldsymbol{B} = \| b_{li} \|_{\substack{i=1,2,\cdots K \\ l=-N,-N+1,\cdots N}}.$$

The linear system defined by (17) can be written in terms of these matrices if we neglect the contribution of modes with order greater than N, this assumption implying the truncation of the infinite series down to $2N+1$ terms. This procedure allows the determination of the mode coefficient vector as

$$\boldsymbol{m} = \frac{j}{2\pi Y_e}\left(\boldsymbol{F} - \frac{\epsilon_2 k_1 R_1}{\pi \epsilon_1}\boldsymbol{T}\boldsymbol{J}\boldsymbol{\Lambda}\right)^{-1}\boldsymbol{B}\boldsymbol{\xi}. \quad (18)$$

Voltage and current at the ith disk reference plane are given by

$$V_{di} = -\frac{h}{2\psi_i}\int_{\gamma_i} E_z^{(1)}(R_1, \phi)\, d\phi \quad (19)$$

$$I_{di} = -4g R_1 \psi_i H_i \quad (20)$$

where $g = 1$ (SD), $1/2$ (MD). Hence, using (2) and (15) in (19)

$$\boldsymbol{v}_d = -\frac{h}{2}\boldsymbol{\Psi}\boldsymbol{B}^+\boldsymbol{J}\boldsymbol{m} \quad (21)$$

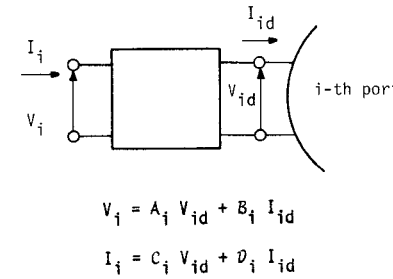

Fig. 4. Transfer parameters ($\mathcal{A}\,\mathcal{B}\,\mathcal{C}\,\mathcal{D}$) of the matching network at ith port.

$$\boldsymbol{\xi} = -\frac{1}{4gR_1}\cdot\boldsymbol{\Psi}\boldsymbol{i}_d. \quad (22)$$

By substituting (22) in (18) and the result in (21), the impedance matrix at the disk ports is obtained as

$$\boldsymbol{Z}_d = jZ_0\boldsymbol{\Psi}\boldsymbol{B}^+\boldsymbol{J}\left(\boldsymbol{F} - \frac{\epsilon_2 k_1 R_1}{\pi\epsilon_1}\boldsymbol{T}\boldsymbol{J}\boldsymbol{\Lambda}\right)^{-1}\boldsymbol{B}\boldsymbol{\Psi}$$

or

$$\boldsymbol{Z}_d = jZ_0\boldsymbol{\Psi}\boldsymbol{B}^+\left(\boldsymbol{F}\boldsymbol{J}^{-1} - \frac{\epsilon_2 k_1 R_1}{\pi\epsilon_1}\boldsymbol{T}\boldsymbol{\Lambda}\right)^{-1}\boldsymbol{B}\boldsymbol{\Psi} \quad (23)$$

where

$$Z_0 = \frac{h}{16\pi g R_1}(\mu_1/\epsilon_1)^{1/2}.$$

We point out that the matrices containing the information about the number of ports, their positions and coupling angles, are completely frequency independent. This lends to (23) a great flexibility, which is useful for design purposes.

Equation (23) clearly shows that $\boldsymbol{Z}_d$ is anti-Hermitean when the fringing fields are neglected ($\boldsymbol{\Lambda} = 0$). In the general case, it is easily verified that the matrix T is Hermitean and that the main diagonal strongly dominates. All the numerical results showed that the elements of the Hermitean part of $\boldsymbol{Z}_d$ were negligible so that the losslessness condition $\boldsymbol{Z}_d + \boldsymbol{Z}_d^+ = 0$ was always approximated with a very high degree of accuracy.

Describing the matching networks by their transfer parameters (Fig. 4), we readily obtain the impedance matrix at the K-port reference planes as

$$\boldsymbol{Z} = (\mathcal{A}\boldsymbol{Z}_d + \mathcal{B})(\mathcal{C}\boldsymbol{Z}_d + \mathcal{D})^{-1} \quad (24)$$

where

$$\mathcal{A} = \mathrm{diag}[\, \mathcal{A}_1, \mathcal{A}_2, \cdots, \mathcal{A}_k \,]$$

and so on.

V. Disk Reactance

In this section an approximate quasi-static formula for the isotropic microstrip disk is presented. The result is compared to more exact methods previously published [10]–[12]. Numerical results, obtained with the inclusion of higher order modes and experimental data for 2 prototypes are also presented.

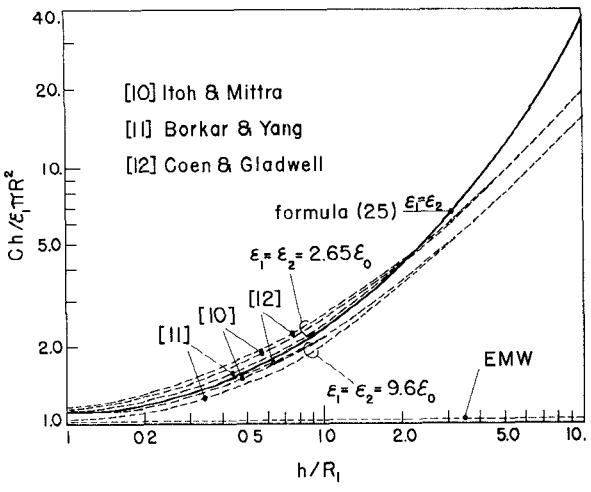

Fig. 5. Microstrip disk capacitance.

For the quasi-static formula, only the zero order aximuthal mode is retained and since $K=1$ all the matrices of (23) become scalars; as follows:

$$\boldsymbol{B}=b_{01},\quad \boldsymbol{F}=F_0,\quad \boldsymbol{J}=J_0,\quad \boldsymbol{T}=T_{00},\quad \boldsymbol{\Lambda}=\Lambda_0$$

with $b_{01}=2\Psi_1$ and $T_{00}=2(\pi-\psi_1)$ as defined by (15) and (16), respectively. With the small argument approximations: $J_0(x)=1$ and $J_1(x)=x/2$, the disk capacitance is obtained from (23) as

$$C=\epsilon_1\frac{\pi R_1^2}{h}\left[1+4\frac{\epsilon_2}{\epsilon_1}\left(1-\frac{\psi_1}{\pi}\right)\Lambda_0\right]. \tag{25}$$

When $R_2\gg h$ and $\Omega\ll\pi/2$, an approximate expression for the zero order fringing function can be found by retaining only the first term in (13):

$$\Lambda_0=\left(\frac{2}{\pi}\right)^3\frac{1}{\hat{R}_1}\frac{K_1(\pi\hat{R}_1/2)}{K_0(\pi\hat{R}_1/2)}. \tag{26}$$

Fig. 5 shows the normalized capacitance, as computed via (25) and (26) for $\psi=0$ and $\epsilon_1=\epsilon_2$, compared to results published in references [10]–[12]. The horizontal dashed line is the result when fringing fields are neglected ($\Lambda_0=0$).

This quasi-static approximation is severely restricted in frequency range due to the appearance of higher order azimuthal modes resonances. This is exemplified in Fig. 6 where experimental data are checked against formula (25) and numerical results obtained with $N=3$ ($n=0,\pm1,\pm2,\pm3$) in (23), with and without fringing fields. Experimental measurements were taken at the end of the input line ($r=R_2$) and transferred to the disk edge. The upper measurement frequency was limited by the appearance of losses. Fig. 7 shows the results for a low dielectric constant stripline disk geometry. It is apparent that the experimental points agree very well with the present theory, while the EMW theory yields considerable error.

In order to illustrate the convergence of numerical results when the number of modes is increased, the input impedance of the disk of Fig. 6 is plotted in Fig. 8, for N ranging from 1 to 3.

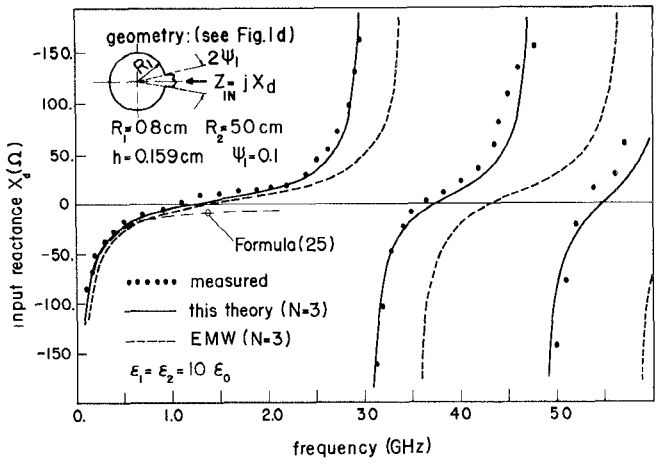

Fig. 6. Experimental microstrip disk input impedance compared to quasi-static formula and to full theory; with and without fringing fields (EMW).

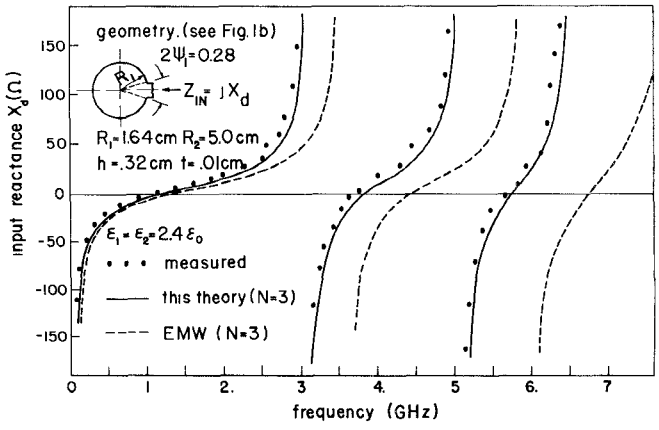

Fig. 7. Experimental stripline disk input impedance compared to theory, as in Fig. 6.

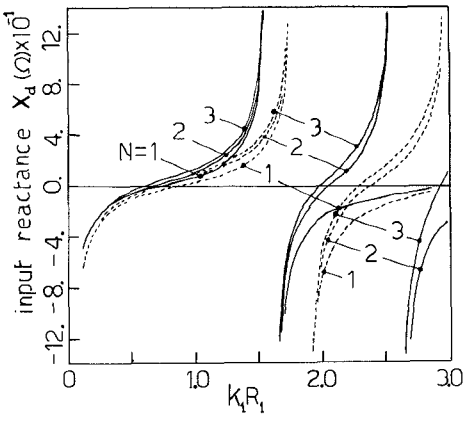

Fig. 8. Convergence of numerical results plotted in Fig. 7 for three different numbers of modes; with and without fringing fields (dashed line).

VI. Reciprocal Transmission Zeros

In order to find the relative position of two ports which are optimal with respect to transmission zero properties the transmission parameter S_{21}, computed from (23), was investigated. To speed computations the fringing function is neglected in the first step where the search for an

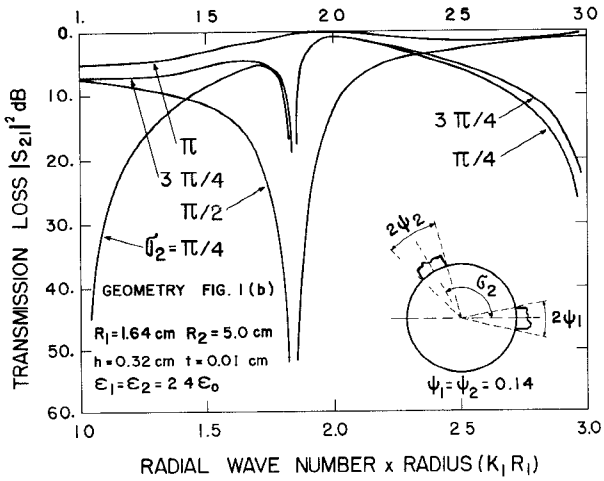

Fig. 9. Transmission loss (relative to 50 Ω) for four different port positions; without fringing fields and for $N=3$.

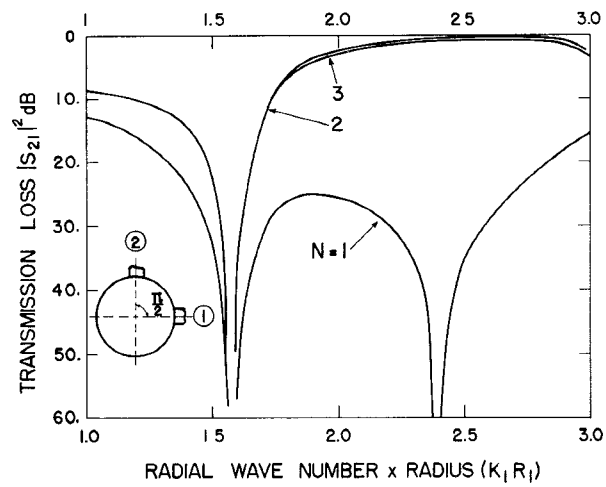

Fig. 10. Transmission loss (relative to 50 Ω) for the 90° 2 port of Fig. 9 and for three numbers of modes; fringing fields included.

optimum port position is done (Fig. 9). It is clear from Fig. 9 that a useful geometry for a band elimination filter is the 90° 2-port disk. Fig. 10 shows the parameter S_{21} for this geometry, computed for $N=1$-3, fringing fields included.

The numerical results of Figs. 9 and 10 for $N=3$ are reproduced in Fig. 11, together with the experimental data.[3]

VII. Conclusions

A self consistent theory for the analysis of a disk n port, which includes the fringing fields and is also applicable to nonreciprocal devices has been developed. Application to the microstrip disk capacitor led to a useful approximate formula that shows good agreement with previously published work. Applicability to numerical design is exemplified with the search of transmission zeros in reciprocal 2-port disks. Numerical results, when compared with

[3]The computation time for the scattering parameters of Fig. 11 was 0.5s, each point, for the complete analysis and 0.3s without fringing fields, in a Burroughs 6.700 machine.

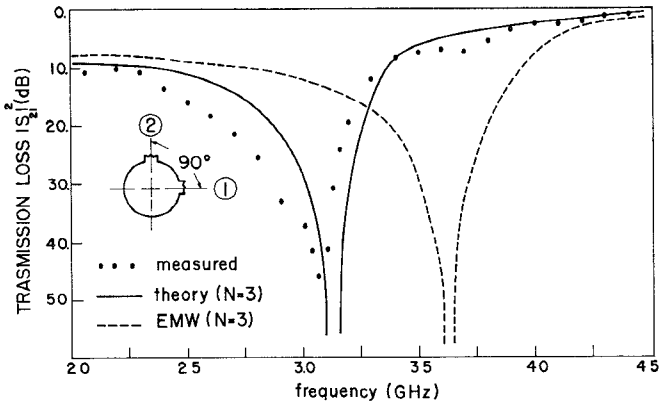

Fig. 11. Experimental band-elimination filter response compared to results of this theory and with those provided by EMW assumption; geometry: stripline disk (Fig. 1(b)) with parameters insert on Fig. 9. The disk is directly coupled to 50-Ω striplines.

those provided by the EMW assumption and with experimental data, show that the inclusion of the fringing fields significantly reduces the error in both impedance levels and resonant frequencies.

VIII. Appendix

The geometry of the structure, together with Maxwell's equations and separation of variables, leads to the following form for the fields in both regions:

$$\boldsymbol{E}^{(i)}(r,\phi,z) = \boldsymbol{E}_t^{(i)}(r,\phi)\sin\beta_i z + E_z^{(i)}(r,\phi)\cos\beta_i z\,\hat{z} \quad \text{(A1)}$$

$$\boldsymbol{H}^{(i)}(r,\phi,z) = \boldsymbol{H}_t^{(i)}(r,\phi)\cos\beta_i z, \qquad i=1,2 \quad \text{(A2)}$$

where $\boldsymbol{E}_t$ and $\boldsymbol{H}_t$ are parallel to the ground plane. Only the modes without RF magnetic field in the z direction are being considered.

Substitution of (A1) and (A2) into Maxwell's equations leads to Helmholtz's homogeneous equation for E_z:

$$(\nabla^2 + k_t^2)E_z^{(i)}(r,\phi) = 0 \quad \text{(A3)}$$

with

$$k_t^2 = \omega^2\mu_i\epsilon_i - \beta_i^2, \qquad i=1,2. \quad \text{(A4)}$$

In cylindrical coordinates (A3) yields the eigenfunctions

$$J_n(k_1 r)e^{-jn\phi}, \qquad \text{for } r \leqslant R_1$$

$$J_n(k_2 r)e^{-jn\phi}, Y_n(k_2 r)e^{-jn\phi}, \qquad \text{for } R_1 \leqslant r \leqslant R_2 .$$

The depth wave number β_i is determined by the boundary conditions

$$\hat{z} \times \boldsymbol{E}^{(i)}(r,\phi,z) = 0$$

with $z=h$ and $2h+t$ for $i=1$ and 2, respectively, for stripline geometry. For the microstrip disk the condition for $\boldsymbol{E}^{(1)}$ is repeated, but, for the outer fields due to the assumed magnetic wall at $z=h$, the boundary condition is

$$\hat{z} \times \boldsymbol{H}^{(2)}(r,\phi,h) = 0.$$

Therefore,

$$\beta_{1m} = m\pi/h \quad \text{(A5)}$$

$$\beta_{2m} = m\pi/(2h+t) \quad \text{(SD)}, \qquad m=0,1,2,\cdots \quad \text{(A6a)}$$

$$\beta_{2m} = m\pi/2h \quad \text{(MD)}, \qquad m=1,3,5,\cdots . \quad \text{(A6b)}$$

The integer m defines the order of the depth mode. The cutoff frequency[4] ω_{im} of the mth depth mode in region i is, from (A4),

$$\omega_{im} = \beta_{im}(\mu_i \epsilon_i)^{-1/2}. \tag{A7}$$

The sign of k_1 and k_2 for the modes below cutoff must be chosen so that the respective eigenfunctions correspond to a decaying field in the radial direction (inwards in medium 1 and outwards in medium 2). This condition leads to the choice of

$$k_i = -j(\beta_i^2 - \omega^2 \mu_i \epsilon_i)^{1/2} \quad \text{when} \quad \omega < \beta_i(\mu_i \epsilon_i)^{-1/2}. \tag{A8}$$

The knowledge of the E_z function allows the determination of the field components through the application of Maxwell's equations to (A1) and (A2). The eigenfunctions of the zeroth order depth mode of region 1 were determined in [5] and are displayed in Section I of this work. For the outer region we obtain

$$E^{(2)}_{\phi nm} = \beta_{2m} k_2^{-2} \frac{\partial E^{(2)}_z}{r \partial \phi} \sin \beta_{2m} z \tag{A9}$$

$$E^{(2)}_{rnm} = \beta_{2m} k_2^{-2} \frac{\partial E^{(2)}_z}{\partial r} \sin \beta_{2m} z \tag{A10}$$

$$H^{(2)}_{\phi nm} = j\omega \epsilon_2 (\beta_{2m} \tan \beta_{2m} z)^{-1} E^{(2)}_{rnm} \tag{A11}$$

$$H^{(2)}_{rnm} = -j\omega \epsilon_2 (\beta_{2m} \tan \beta_{2m} z)^{-1} E^{(2)}_{\phi nm} \tag{A12}$$

where $E_z^{(2)}(r,\phi) = C_n(K_2 r) e^{-jn\phi}$ and the C_n are linear combinations of the radial eigenfunctions J_n and Y_n, displayed in Table I, chosen so as to satisfy the boundary condition at $r = R_2$ for either the electric or magnetic wall. For numerical purposes, the special Bessel functions are used when k_2 is imaginary.

Nomenclature

r, ϕ, z	Cylindrical coordinates.
R_1, R_2	Disk and outer dielectric radii.
γ_i, Γ_i	Sectors of disk edge.
$2\psi_i$	Coupling angle at ith port.
h	Disk to ground plane spacing.
t	Stripline disk conductor thickness.
$\hat{R}_1, \hat{R}_2, \hat{t}$	Normalized quantities with respect to h.
μ, κ	Diagonal and off-diagonal elements of the Polder tensor [13].
ϵ_i, μ_i	Permittivity and effective permeability of region i ($i = 1,2$) with $\mu_1 = (\mu^2 - \kappa^2)/\mu$ and $\mu_2 = \mu_0$.
Y_e	Intrinsic wave admittance of region 1.
β_i, k_i	Depth and radial wave numbers.
Ω	Normalized frequency.
J_n, Y_n	Bessel functions of first and second kind and order n.
I_n, K_n	Special Bessel functions of first and second kind.
$\sum_n$	Summation over all integers.
$\sum_m$	Summation over all nonnegative integers, unless otherwise specified.
H_i	Azimuthal component of RF magnetic field at ith port.
EMW	Edge magnetic wall boundary condition.
(SD)	Relative to stripline disk geometry.
(MD)	Relative to microstrip disk geometry.
Depth modes	z-dependent modes.

[4]The frequency at which radially oscillatory fields transform into decaying fields and vice versa.

Acknowledgment

We wish to thank the unknown reviewers, whose suggestions greatly contributed to the clarity of this paper.

References

[1] P. P. Civalleri and S. Ridella, "Impedance and admittance matrices of distributed rectangular structures," *IEEE Trans. Circuit Theory*, vol. CT-17, pp. 392–398, Aug. 1970.

[2] T. Okoshi and T. Miyoshi, "The planar circuit—An approach to microwave integrated circuitry," *IEEE Trans. Microwave Theory Tech.*, vol. MTT-20, pp. 245–252, Apr. 1972.

[3] P. Silvester, "Finite element analysis of planar microwave networks," *IEEE Trans. Microwave Theory Tech.*, vol. MTT-21, pp. 104–108, Feb. 1973.

[4] T. Miyoshi, S. Yamaguchi, and S. Goto, "Ferrite planar circuits in microwave integrated circuits," *IEEE Trans. Microwave Theory Tech.*, vol. MTT-25, pp. 593–600, July 1977.

[5] H. Bosma, "On stripline Y-circulation at UHF," *IEEE Trans. Microwave Theory Tech.*, vol. MTT-12, pp. 61–72, Jan. 1964.

[6] C. E. Fay and R. L. Comstock, "Operation of the ferrite junction circulator," *IEEE Trans. Microwave Theory Tech.*, vol. MTT-13, pp. 15–27, Jan. 1965.

[7] Y. S. Wu and F. J. Rosenbaum, "Wide-band operation of microstrip circulators," *IEEE Trans. Microwave Theory Tech.*, vol. MTT-22, pp. 849–856, Oct. 1974.

[8] H. Bosma, "Junction Circulators," *Advances in Microwaves*, vol. 6, L. Young, Ed. New York: Academic Press, 1971.

[9] P. de Santis, "High-azimuthal-index resonances in ferrite MIC disk resonators," *IEEE Trans. Microwave Theory Tech.*, vol. MTT-25, pp. 360–367, May 1977.

[10] T. Itoh and R. Mittra, "A new method for calculating the capacitance of a circular disk for microwave integrated circuits," *IEEE Trans. Microwave Theory Tech.*, vol. MTT-21, pp. 431–432, June 1973.

[11] S. R. Borkar and R. F. H. Yang, "Capacitance of a circular disk for applications in microwave integrated circuits," *IEEE Trans. Microwave Theory Tech.*, vol. MTT-23, pp. 588–591, July 1975.

[12] S. Coen and G. M. L. Gladwell, "A legendre approximation method for the circular microstrip disk problem," *IEEE Trans. Microwave Theory Tech.*, vol. MTT-25, pp. 1–6, Jan. 1977.

[13] D. Polder, "On the theory of ferromagnetic resonance," *Phil. Mag.*, vol. 40, pp. 99–115, Jan. 1949.